Biomaterials 156 (2018) 159–171

Contents lists available at ScienceDirect

Biomaterials

journal homepage: www.elsevier.com/locate/biomaterials

Soft chitosan microbeads scaffold for 3D functional neuronal networks

Maria Teresa Tedesco [a, 1], Donatella Di Lisa [a, 1], Paolo Massobrio [a], Nicolò Colistra [a], Mattia Pesce [b], Tiziano Catelani [c], Elena Dellacasa [a], Roberto Raiteri [a, d], Sergio Martinoia [a, d], Laura Pastorino [a, *]

[a] University of Genova, Dept. of Informatics, Bioengineering, Robotics and System Engineering, Via Opera Pia 13, 16145, Genova, Italy
[b] Nanoscopy and Nikon Centre, Istituto Italiano di Tecnologia, via Morego, 30, 16163, Genova, Italy
[c] Electron Microscopy Facility, Istituto Italiano di Tecnologia, via Morego, 30, 16163, Genova, Italy
[d] CNR - Institute of Biophysics, Via De Marini, 6, 16149, Genova, Italy

ARTICLE INFO

Article history:
Received 31 July 2017
Received in revised form
15 November 2017
Accepted 27 November 2017
Available online 28 November 2017

Keywords:
Chitosan
Microbeads
Neuronal culture
3D network
Micro-electrode arrays (MEAs)

ABSTRACT

The availability of 3D biomimetic *in vitro* neuronal networks of mammalian neurons represents a pivotal step for the development of brain-on-a-chip experimental models to study neuronal (dys)functions and particularly neuronal connectivity. The use of hydrogel-based scaffolds for 3D cell cultures has been extensively studied in the last years. However, limited work on biomimetic 3D neuronal cultures has been carried out to date. In this respect, here we investigated the use of a widely popular polysaccharide, chitosan (CHI), for the fabrication of a microbead based 3D scaffold to be coupled to primary neuronal cells. CHI microbeads were characterized by optical and atomic force microscopies. The cell/scaffold interaction was deeply characterized by transmission electron microscopy and by immunocytochemistry using confocal microscopy. Finally, a preliminary electrophysiological characterization by micro-electrode arrays was carried out.

© 2017 Elsevier Ltd. All rights reserved.

1. Introduction

The physico-chemical characteristics of the extracellular matrix (ECM) play a fundamental role in regulating relevant physiological cellular processes and in different pathological situations [1,2]. Consequently, it has become clear that cellular organization in 3D is crucial to study biological functions [3,4]. To date, most *in vitro* functional studies have been performed using oversimplified traditional monolayer cultures. However, in the last few years, a growing number of research groups have been focusing on the setting up of cellular models which mimic the in *vivo* microenvironment at a higher extent [5,6]. This approach This approach has proven to be essential to gain information on pathological processes like cancer, where cell-cell and cell-microenvironment interactions play a major role [7]. The availability of 3D culture platforms, specifically designed to mimic different tissues towards the development of organ-on-a-chip [8], is expected to have a strong impact not only in the study of physiological and pathological processes, but also in drug screening and in toxicity assays [3,9–13]. In the process of developing 3D *in vitro* models, a fundamental step is represented by the engineering and tailoring of a 3D matrix containing adequate chemical and mechanical signals in order to support the cell phenotypes of interest. In this respect, synthetic and natural hydrogels have been used to develop 3D models for soft tissues, because of hydrophilicity, biocompatibility, biodegradability, and tunable microporosity [11,14–21]. Among soft tissue models, 3D interconnected networks of neuronal cells are very useful to investigate in a reduced *in vitro* model, neuronal (dys)functions and connectivity for applications ranging from basic neuroscience to drug screening [22–24].

Under this perspective, we have recently demonstrated that 3D hippocampal networks, made by self-assembled glass microbeads as scaffold, and coupled to micro-electrode arrays (MEAs), represent a suitable *in vitro* model for neurophysiological studies alternative and complementary to the classical 2D neuronal network models [25]. Matrix stiffness and composition are the most critical properties, since they can influence growth dynamics, synaptic density, and electrophysiological activity of the neuronal network [26–28]. In this work, we propose the use of soft porous hydrogel microbeads platform, mimicking the physico-chemical characteristics of the ECM, for the growth of 3D neuronal networks. Natural

* Corresponding author.
E-mail address: laura.pastorino@unige.it (L. Pastorino).
[1] M.T. and D.D.L. contributed equally to this work.

https://doi.org/10.1016/j.biomaterials.2017.11.043
0142-9612/© 2017 Elsevier Ltd. All rights reserved.

soft materials used in 3D neuronal cell culture have been mainly based on the use of proteins, such as collagen [29,30], or of ECM protein mixtures, such as Matrigel™ matrix [6,31].

In the last few years, polysaccharides have been proposed and widely used as biomimetic materials for scaffold fabrication for a huge variety of cell types [32,33]. However, the use of polysaccharides for 3D neuron cultures has been quite limited as compared to other cell types. Among the polysaccharides, alginate, hyaluronic acid, and gellan gum have been mainly investigated [34–37]. Very few studies have addressed the use of chitosan, and the electrophysiological behavior of chitosan based 3D neuronal cultures is still unknown [38–46]. Chitosan is a copolymer of glucosamine and N-acetyl-glucosamine, obtained by the deacetylation of chitin, which is the main component of crustacean and insect exoskeletons [47]. Chitosan can behave as a polycation under acidic conditions (pH < 6), due to the protonation of free amino groups [48]. This polysaccharide is well known for its biocompatibility, biodegradability, muco-adhesiveness, and antibacterial and antifungal activity [49]. Interestingly, as previously demonstrated, chitosan enhances neuron attachment, proliferation and neurite extension, and exerts a potent neuroprotective action [50,51]. The aim of this study was to explore the use of chitosan as scaffold material for 3D neuronal networks coupled with MEAs.

As a first step, 2D physically cross-linked chitosan films were prepared by phase inversion (liquid to solid) in an ethanol/sodium hydroxide solution [52] and their interaction with neurons was assessed by inverted microscopy, with and without treatment with adhesion proteins. The 2D cultures carried out onto chitosan films were investigated only in the view of gaining information on the bioactivity of chitosan in terms of cell adhesion ad network development. Physically cross-linked chitosan microbeads were then fabricated by an aerodynamically-assisted jetting technique, characterized by optical and atomic force microscopies (AFM) and then used as scaffold for 3D hippocampal neuron cultures. The 3D neuronal networks were characterized morphologically by transmission electron microscopy (TEM), by immunofluorescence techniques and 3D imaging with a confocal microscope. The spontaneous electrophysiological activities of the obtained 3D networks were recorded after 21 days of *in vitro* culture (21 DIV); results were compared with those obtained using glass microbeads [25] as 3D scaffold for neuronal growth.

2. Materials and methods

2.1. Preparation of chitosan films

Chitosan (CHI, medium molecular weight, 75–85% deacetylated, code 448877, lot MKBD4275V, from Pandalus Borealis), ethanol, sodium hydroxide and acetic acid were purchased from Sigma-Aldrich.

CHI was dissolved in 0.1 M acetic acid under continuous stirring for 2 h and filtered through a syringe filter (5 μm) to remove any undissolved material. Films were prepared from CHI solutions at concentrations 1% and 2% w/v. CHI solutions (1 ml) were poured on a petri dish (⌀35 mm) and allowed to dry before exposing them to 1 ml of gelling solution overnight. The gelling solution was prepared by mixing H_2O_{dd} 40%, Ethanol 60% and NaOH 2% w/v. The gelling solution composition was optimized on the basis of the data present in the literature and on results obtained by the FT-IR characterization of CHI samples crosslinked at different concentrations of NaOH (data not shown) [53,54]. The obtained films were washed several times with distilled water.

2.2. Preparation of chitosan microbeads

Two CHI concentrations were tested for microbeads fabrication, namely 1% and 2% w/v. 3 ml of filtered CHI solutions were extruded using a microencapsulation unit (Nisco Encapsulation Unit VAR J30) equipped with a conical nozzle having a diameter of 0.25 mm [52]. The extrusion flow rate was 0.4 ml/min under 100 mbar pressure for CHI 1%, whereas for CHI 2% the extrusion flow rate was 0.5 ml/min under 200 mbar pressure. The generated microdroplets were collected into 150 ml of gelling solution bath while continuously stirring at 200 rpm. The distance from the nozzle to the gelling solution was set at 6 cm. The resulting microbeads were left in contact with the gelling solution for 30 min at room temperature to ensure complete solidification. Afterwards, the gelling solution was removed through centrifugation (1000 rpm for 5 min), followed by four washing steps in distilled water. The production yield was evaluated using optical microscopy. An inverted optical microscope (IX-51 Olympus microscope equipped with a DP70 digital camera and with a 10× N.A. 0.25 PhC objective) was used to take images of the microbeads. From the collected images, after binarization, the “analyze particles tool” of ImageJ software (NIH, USA) was used to evaluate the projected areas of the microbead. Areas of particles touching each other were separated by watershed segmentation.

2.3. Characterization of chitosan microbeads

The mean particle size and size distributions were evaluated using optical microscopy. The mean particle size was evaluated using ImageJ software as described above.

2.3.1. Water content

2.5×10^6 microbeads in 0.5 ml of water were weighed inside an Eppendorf tube and were then lyophilized. The weight of the dried microparticles was measured and the water content was calculated using the following equation, where Ws is the weight of hydrated microbeads and Wd is the weight of the lyophilized ones:

$$\text{Water content} = \frac{(Ws - Wd)}{Ws} \times 100\%$$

2.3.2. Atomic force microscopy (AFM)

A commercial atomic force microscope, equipped with a closed loop scanner capable of 9 μm vertical range (Keysight Technologies, model 5500ILM), was used to measure both the topography and the stiffness of the microbeads. Rectangular micro-cantilevers (Mikromash HQ:CSC38, type B, nominal spring constant k = 0.03 N/m) either with a conical tip or without any tip were employed. Images of the topography of single beads were obtained in contact mode, by careful adjusting the lowest possible force to keep the contact during the whole scan. In order to evaluate the stiffness of the beads, standard force curves were recorded and the region after contact was considered for further analysis. The applied load for cantilever deflections was calculated by first converting the output voltage, from the AFM four-segment photodetector, into nanometers of deflection, and then by multiplying the deflection by the cantilever spring constant. The conversion factor was calculated by taking several force curves onto a hard glass substrate each time the laser spot on the cantilever had to be adjusted, and by considering the reciprocal of the average slope of the constant compliance region of the curves. When using sharp conical tips, the load versus indentation curve was evaluated to extract the elastic modulus of the sample using the model proposed by Oliver and Pharr [55] as

already described in Ref. [56]. When using tipless cantilevers the load versus microbead deformation curve was evaluated in order to extract the stiffness of the bead in analogy with unconfined compression testing. All measurements were performed at a constant approaching/retracting speed of 1 μm/s. This allowed us to compare results, despite the viscous (*i.e.* speed-dependent) response of the CHI microbeads. In order to take into account intra-sample heterogeneity, 16 × 16 = 256 force curves were recorded over a regular grid over a 5 × 5 μm.

Microbeads were adsorbed onto the surface of a petri dish premodified by the deposition of a layer of polyethylenimine (PEI 1 mg/ml in pure water, from Sigma Aldrich), followed by a layer of polystyrene sulfonate (PSS 2 mg/ml, Sigma-Aldrich). For both samples, three maps of 16 × 16 curves were collected onto three different microbeads randomly selected over the petri surface.

2.4. Cell preparation

Hippocampi were dissected and removed from embryonic Sprague-Dawley rats at gestational day 18 under sterile conditions. Hippocampal fetal tissue was enzymatically digested in Trypsin 0.125% in Ca^{++} and Mg^{++} free Hank's (Gibco Invitrogen) for 20′ at 37 °C. The enzymatic process was quenched by adding culture medium supplemented with 10% of FBS (Sigma-Aldrich) then the tissue was mechanically dissociated with a smoothly fire-polished Pasteur pipette. Neurons were re-suspended in plating medium consisting of Neurobasal medium (Gibco Invitrogen) with 2% w/v B-27 Supplement (Gibco Invitrogen), 1% Glutamax (Gibco Invitrogen), 1% Pen-Strepto (Gibco Invitrogen). Cultures were maintained in incubator at 37 °C in a 5% CO_2, 95% humidity atmosphere for 3–4 weeks by replacing half of the medium once a week [57]. The experimental protocol was approved by the European Animal Care Legislation (2010/63/EU), by the Italian Ministry of Health in accordance with the D.L. 116/1992 and by the guidelines of the University of Genova. All efforts were made to reduce the number of animals used for the project and to minimize their suffering [58].

2.4.1. Preparation of 2D networks on CHI films and 3D networks on CHI microbeads

The day before plating, CHI films and microbeads were sterilized by exposure to ethanol 70% for 2 h. The sterilized samples were then washed with sterile water 5 times, normalized in cell culture medium and used for the cell culture experiments. To evaluate the bioaffinity between CHI and neurons, cultures were prepared using both films and microbeads treated and untreated with adhesion proteins (a.p.).

In the first case, both films and microbeads were exposed to a mix of a. p., namely Laminin:P-D-Lysine (1:1), at the concentration of 0.05 mg/ml in sterile water (L-2020; P-6407 Sigma-Aldrich) and left in the incubator overnight at 37 °C. The a. p. were then washed away from the films with sterile water, while the microbeads were centrifuged three times, for 5 min at 1000 rpm. Each centrifugation step was followed by a washing step in sterile water. In the second case, both films and microbeads were sterilized and used without any further treatment. Before cell plating, both films and microbeads were washed in a Neurobasal medium. Hippocampal neurons were plated onto the film surface at a seeding concentration of 1000 cell/μl with a final cell density of 800 cell/mm^2. In the case of cell plating onto the microbead surface, the microbeads were exposed to the cell suspension in complete Neurobasal medium; the ratio of the number of microbeads to the number of neurons was nominally 1:4. Eppendorf vials were used for this step; 10^6 microbeads/ml and 4 × 10^6 cells/ml were mixed and after an interval of around 3–4 h they aggregated and formed small clusters. The vials were kept in horizontal position and turned for 12–16 times at 20–25 min intervals in order to expose the whole microbead surface to the suspended cells. At the end of the incubation-adhesion phase, the neuron-microbead aggregates were left to deposit slowly at the bottom of the vial. Finally, they were carefully collected with a micropipette in small volumes (30–35 μl), and directly transferred onto standard petri dishes (⌀35 mm) for subsequent immunocytochemistry characterization, or plated onto the MEA surface for electrophysiological characterization.

The day before plating, MEAs were assembled with donuts-shaped Poly-dimethyl-siloxane (PDMS) structures (internal and external diameters: 5 and 22 mm respectively, height: 650 μm) to confine the self-assembled microbeads and neurons onto a circular surface of ~20 mm^2 around the active electrodes area (Fig. 1A). MEAs (assembled as explained above) were sterilized in the oven at 120° for 2 h. At the end of the sterilization process, the chips were treated only on the area delimited by the PDMS structure, with a mix of a. p. namely Laminin: P-D-Lysine (1:1), at the concentration of 0.05 mg/ml in sterile water (L-2020; P-6407 Sigma) and left in the incubator overnight at 37 °C. The coating solution was removed from the MEA which was then washed twice with water and left to dry under the laminar hood until the plating took place. Similarly to what performed in Ref. [25], hippocampal neurons without microbeads were first plated onto the MEA surface to create a first monolayer of cells at a final concentration of 800–1000 cell/mm^2. 3–4 h after plating, 30–35 μl of neuron-microbead aggregates were transferred inside the PDMS confinement structure onto the area on which hippocampal neurons were previously seeded (Fig. 1B).

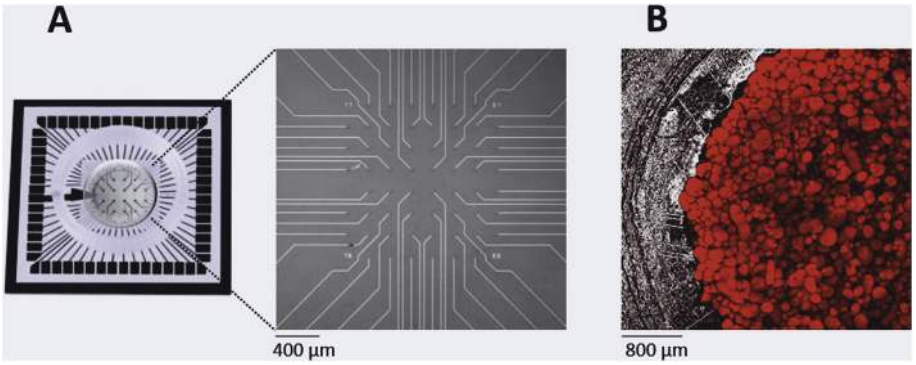


Fig. 1. Set-up configuration: (**A**) Micro-electrode arrays (MEAs) made up of 60 planar microelectrodes (TiN/SiN, 30 μm electrode diameter, 200 μm spaced) arranged over an 8 × 8 square grid with inserted PDMS (internal diameter 5 mm) constraint on the active area; (**B**) 3D CHI scaffold macroscale assembly onto MEA labeled for MAP-2.

Around 4.5×10^4 microbeads and 1.5×10^5 cells were transferred into MEAs.

2.5. Morphological characterization of 3D neuronal networks by transmission electron microscopy

In order to analyze the samples with Transmission Electron Microscopy (TEM), the 3D networks on CHI 2% were fixed for 2 h in a fixative solution (2% Glutaraldehyde, in buffer Na-Cacodylate 0.1 M) and then post-fixed (2 h) in a solution 1% OsO4, 1,5% Potassium Hexacyanoferrate, in Na-cacodylate buffer 0.1 M. Subsequently, they were stained overnight in a 1% Uranyl acetate aqueous solution and dehydrated with series of alcohols. TEM samples were infiltrated with Propylene Oxide and low viscosity Spurr resin (SPI-Chem). Once the resin hardened, 70 nm thick sections were cut with a Leica EMU C6 ultra-microtome. TEM images were collected by means of Jeol JEM 1011 (Jeol, Japan) TEM, operating at an acceleration voltage of 100 kV, and recorded with a 11 Mp fiber optical charge-coupled device (CCD) camera (Gatan Orius SC-1000). All used reagents were from Sigma-Aldrich.

2.6. Morphological characterization of neuronal networks by immunocytochemistry

To assess the expression of specific neuronal markers, hippocampal cultures were fixed in 4% paraformaldehyde in phosphate buffer solution (PBS), pH 7.4 for 30 min at room temperature. Permeabilization was achieved with PBS containing 0.5% Triton-X100 for 15 min at room temperature and non-specific binding of antibodies was blocked with an incubation of 45 min in a blocking buffer solution consisted of PBS, 0.3% BSA (bovine serum albumin Sigma) and 0.5% FBS. Cultures were incubated with primary antibody diluted in PBS Blocking buffer for 2 h at room temperature or incubated at 4 °C overnight in a humidified atmosphere. Cultures were rinsed three times with PBS and finally exposed to the secondary antibodies. The following primary antibodies were used for CHI films: MAP-2 1:500 (monoclonal or polyclonal Synaptic System), TUBULIN βIII, clone TU-20 (similar TUJ1) 1:500 (Chemicon Millipore), NeuN 1:200 (Chemicon millipore), VGAT and VGLUT1 1:500 (Synaptic System), Synapsin 1:200 (Synaptic System), Dapi 1:10000 (Sigma). The following primary antibodies were used for CHI microbeads: MAP-2 1:500 (monoclonal or polyclonal Synaptic System), TUBULIN βIII, clone TU-20 (similar TUJ1) 1:500 (Chemicon Millipore), NeuN 1:200 (Chemicon Millipore), Dapi 1:10000 (Sigma). To verify the presence of glial cells in the culture, we fixed and exposed to the marker GFAP 1:500 (CHI microbeads) or 1:1000 (CHI films) monoclonal or polyclonal antibodies (Sigma). Cultures were rinsed twice with PBS and finally exposed to the secondary antibodies: Alexa Fluor 488, Alexa Fluor 549, Alexa Fluor 633 Goat anti mouse or Goat anti rabbit, diluted 1:700 and 1:1000 (Invitrogen Life Technologies S. Donato Milanese).

To observe the perineuronal net-like structure, we exposed samples to Wisteria floribunda 1:200 (Sigma-Aldrich) as primary antibody for 24 h and Streptavidin Alexa Fluor 488, 1:700 (Invitrogen Life Technologies S. Donato Milanese) for 6 h as secondary antibody.

A table of all used antibodies and respective dilutions is reported in Supplementary materials (Table S1).

2.6.1. Optical microscopy and confocal imaging

An inverted IX-51 Olympus microscope equipped with a DP70 digital camera coupled with CPlan 10× N.A. 0.25 PhC objective was used to acquire contrast phase images of CHI microbeads coupled with neurons. An Olympus BX-51 upright microscope was used for immunofluorescence evaluation of the biological samples and the image acquisition was done with a Hamamatsu Orca ER II digital cooled CCD camera driven by Image ProPlus software (Media Cybernetic).

Confocal imaging was acquired on two different microscopes: Leica TCS SP5 AOBS Tandem DMI6000 inverted microscope coupled with objective Leica IRAPO 25×, 0.95 NA (Leica Microsystems, Mannheim, Germany) and Leica TCS SP5 AOBS Tandem DM6000 upright microscope coupled with objective Leica IRAPO 25×, 0.95 NA (Leica Microsystems Srl, Italy). Data were analyzed by means of the LASX V2.0 software (Leica Microsystems Srl, Italy).

2.7. MEA recording and analysis

The spontaneous electrophysiological activity of 3D hippocampal neuronal networks was recorded at 21–24 days *in vitro* (DIV) by means of micro-electrode arrays (MEAs) made up of 60 planar microelectrodes (TiN/SiN, 30 μm electrode diameter, 200 μm spaced) arranged over an 8 × 8 square grid (except the four electrodes at the corners), supplied by Multi Channel Systems (MCS, Reutlingen, Germany). The electrophysiological activity was acquired with the 2100 System (MEA 2100-System, MCS), and signals were sampled at 10 kHz. Recordings were performed for 30 min outside the incubator at a temperature of 37 °C. To prevent evaporation and changes of the pH medium, a slow flow of humidified gas (5% CO_2, 20% O_2, 75% N_2) was constantly delivered during the measurement sessions into a small plastic box covering the experimental MEA setup.

2.7.1. Data and statistical analysis

Data analysis was performed by using a custom software package named SPYCODE [59], developed in MATLAB (The Mathworks, Natick, MA, USA). Spike detection was performed by using the Precise Timing Spike Detection (PTSD) algorithm [60]. The algorithm requires three parameters: a different threshold set to 8 times the standard deviation of the baseline noise, a peak lifetime period (set at 2 ms) and a refractory period (set at 1 ms). To characterize the electrophysiological activity, we extracted some first order statistics. In particular, we evaluated the *mean firing rate* (MFR), i.e., the number of spikes per second of each channel and the *percentage of random spikes*, i.e., the fraction of spikes outside bursts. We also performed burst detection according to the method described in Ref. [61]. A burst is a sequence of spikes having an ISI (inter-spike interval, i.e., time intervals between consecutive spikes) smaller than a reference value (set at 100 ms in our experiments), and containing at least a minimum number of consecutive spikes (set at 5 spikes). The parameters extracted from this analysis are the *mean bursting rate* (MBR) and the *mean burst duration* (MBD), which are the frequency and the duration of the bursts at the single channel level respectively. The same approach used for the detection of bursts was applied for the detection of quasi synchronous events at network level called network bursts [59]. The extracted parameters are the *network bursting rate* (NBR) and the *network burst duration* (NBD). NBR computes the number of network bursts per minute, while NBD is the temporal extension of these events.

Statistical analysis was carried out using OriginPro 8 (OriginLab Corporation, Northampton, MA, USA). All data are presented as mean ± standard error of the mean. Statistical analysis was performed using a non-parametric Kruskal-Wallis test, since data do not follow a normal distribution (evaluated by the Kolmogorov-Smirnov normality test). Differences were considered statistically significant when $p < 10^{-3}$. In order to determine which of the sample pairs are significantly different, post-hoc test, using Dunn's test, has been applied.

3. Results

3.1. Preparation and characterization of CHI microbeads

CHI films were investigated only in view of gaining information on the bioactivity of CHI itself. Physically cross-linked CHI films were thus prepared onto petri dishes and the growth of a 2D neuronal network on top of CHI films was characterized. Relevant results are discussed in section 3.2.

1% and 2% CHI microbeads were prepared and characterized in view of their use as scaffolds for neuronal growth. The instrumental parameters, for microbeads production, were optimized in order to promote the formation of the micro-droplet spray and to avoid aggregation of microbeads on the air/gelling solution interface. The production yields were evaluated to be around 0.9×10^6 and 0.7×10^6 per batch for 1% and 2% CHI respectively.

Optical microscopy images of the obtained samples were acquired and analyzed. The results indicated a spherical shape and a size ranging from 40 to 90 μm, with an average diameter of 66 ± 20 μm, for CHI 1%, while for CHI 2% the size ranged from 40 to 160 μm, with an average diameter of 100 ± 40 μm, Fig. 2A–B. Water content values were found to be 98.4% and 99.3% for 2% and 1% CHI microbeads, respectively.

AFM topography showed nanometer sized features onto a rounded profile. The elastic modulus of the microbeads was first evaluated by AFM indentation measurements using microcantilevers with conical tips. The elastic modulus measured on 2% CHI microbeads was in the range 15–25 kPa, whereas 1% chitosan microbeads were too soft to reliably determine the point of contact and, thus, to calculate the elastic modulus. Therefore, we used a tipless cantilever of the same type to press against a single microbead. The slope of the force curve after contact resulted constant for a wide range of applied forces (1–10 nN) and with negligible hysteresis between loading and unloading (Supplementary Materials Fig. S1). This slope represents the stiffness of the microbeads. Stiffness values obtained from the constant compliance region of curves performed on different microbeads using the same cantilever and the same approach-retract speed can be directly compared. In Fig. 2D average stiffness values measured on 1% and 2% CHI microbeads are plotted. The values are normalized versus the average stiffness of 2% CHI beads. 1% microbeads were found to be, on average, 18 fold softer than the average stiffness of the probed 2% microbeads. Interestingly enough, the range of the elasticity value for 1% CHI microbeads that can be inferred by our measurements (1/18 of 15–25 kPa) falls in the same range of reported elasticity values for brain tissue (0.7–1 kPa) [62,63] (see also Supplementary Materials).

3.2. Preparation and characterization of 2D neuronal networks on CHI films

As a first step, the bioaffinity of CHI towards neurons was characterized. To conduct this study, a simplified standard 2D culture model was adopted and cells were thus plated onto the surface of CHI films. In order to evaluate the ability of physically cross-linked CHI to promote neuronal adhesion and development, films both untreated and treated with a. p. were used. Fig. 3 shows the images of neuronal networks developing onto (A) 2% CHI untreated film, (B) 2% CHI film treated with a. p. and (C) petri dish untreated

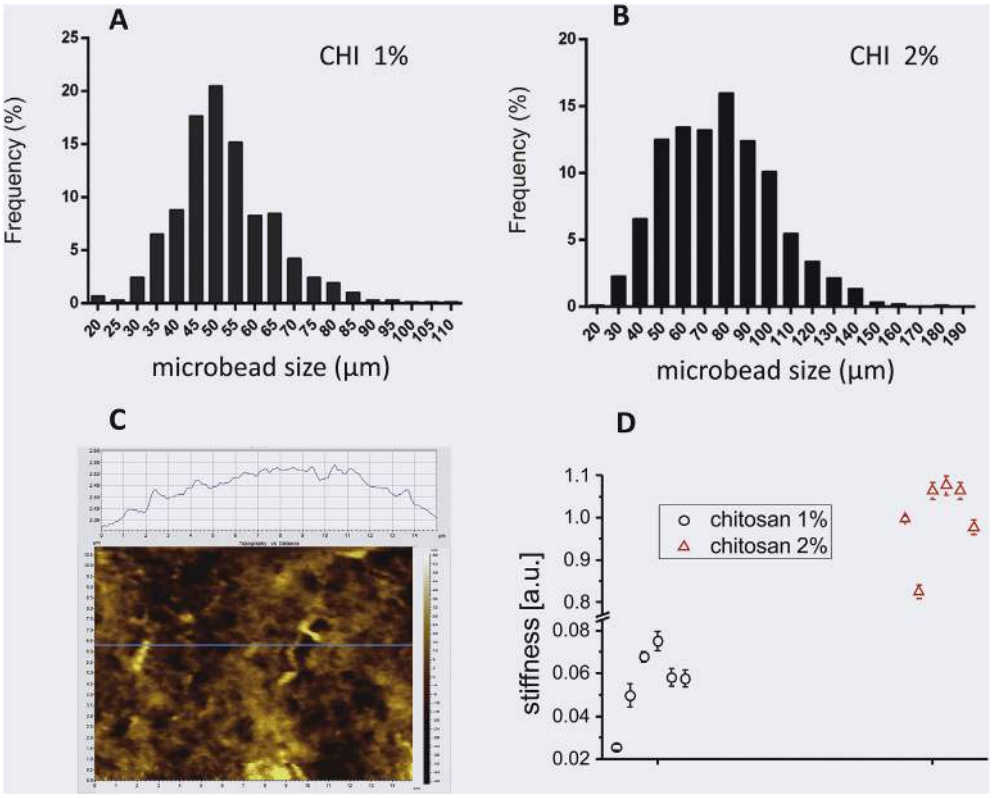


Fig. 2. Characterization of CHI microbeads: (**A**) Histogram of the distribution of CHI 1% microbeads size; (**B**) Histogram of the distribution of CHI 2% microbeads size; (**C**) Topography AFM image (second order flattened) of 15 × 15 μm^2 of a single 2% CHI microbead in culture medium, the insert shows the profile of the raw data from a single line (blue line); (**D**) Stiffness values measured by AFM on 1% and 2% CHI microbeads. (For interpretation of the references to colour in this figure legend, the reader is referred to the web version of this article.)

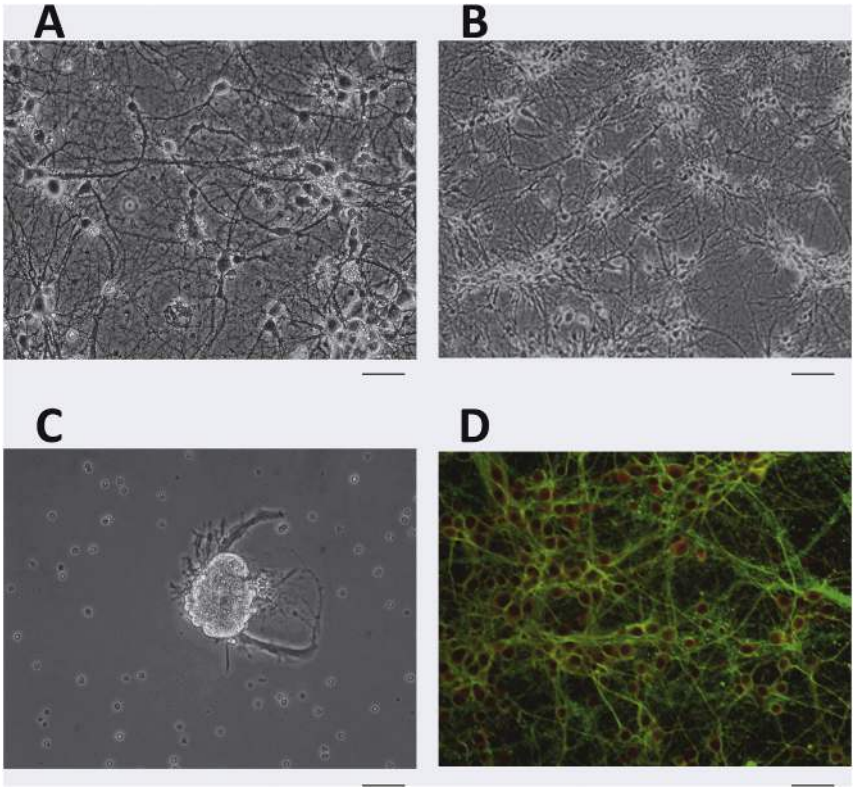


Fig. 3. Optical contrast phase images of 2D neuronal network: (**A**) 2% CHI film untreated with a. p. at DIV 15; (**B**) 2% CHI film treated with a. p at DIV 15; (**C**) petri dish untreated with a. p. at DIV 15; (**D**) 2% CHI untreated film labeled for Tubulin-βIII (green) and NeuN (red) at DIV 25; Scale bar: 50 μm. (For interpretation of the references to colour in this figure legend, the reader is referred to the web version of this article.)

with a. p at DIV 15 and (D) 2% CHI untreated film labeled for Tubulin-βIII and NeuN at DIV 25.

With respect to the morphological development of the neuronal network, it can be observed that cell morphology is similar when cells are plated onto untreated and treated 2% CHI films (Fig. 3A and B). Same results were obtained for cells cultured onto 1% CHI films (data not shown). In Fig. 3C, considered as the negative control, neurons, as expected, tended to form clusters and no network was obtained. Cells showed a homogeneous distribution and the formation of a dense network onto 2% CHI untreated film even at DIV 25 (Fig. 3D). Moreover, the presence of functional structures at DIV 25 was evaluated by 2D networks on 2% CHI film labeled for Synapsin and VGAT-VGLUT (Supplementary Materials Fig. S2). These results confirm that CHI naturally promotes adhesion, neurite growth and structural development of the network, even without any treatment with a. p. Overall, both treated and untreated films were able to sustain the growth and development of cells over three-four weeks, with the formation of a stable network.

In order to quantify the composition of the cellular population during the *in vitro* network development on untreated film, a percentage variation of both the neuronal and glial population has been evaluated (Supplementary Materials Fig. S3).

3.3. Preparation and characterization of 3D neuronal networks on CHI microbeads

As a first step, in order to verify the bioaffinity of CHI also in the form of microbeads, cells were cultured onto CHI microbeads both untreated and treated with a. p. The obtained 3D cultures were observed by contrast phase optical microscopy during the first two weeks of culture in vital conditions. In both cases, a branched and entangled expression of neurites and the presence of healthy neurons, which was demonstrated by the refractivity of the neuronal soma, were observed.

All subsequent experiments were carried out onto 3D neuronal networks grown onto 1% and 2% CHI microbeads pre-treated with a. p. This was done in order to compare the properties of the 3D networks grown onto CHI microbeads with the ones grown onto glass microbeads as described in Ref. [25]. TEM characterization was carried out in order to appreciate the interaction between CHI microbeads and cultured cells. From low magnification imaging (Fig. 4A) it is clear that cells and microbeads (marked with black asterisks) create a dense network. Because of the electron microscopy staining, cell bodies and dendrites appear darker compared to the microbeads, allowing to observe that cells both envelop and penetrate the chitosan scaffold. Higher magnification images show more in detail the interaction among neurons and CHI microbeads. Fig. 4B shows a neuronal cell and its axon pushing out between two beads, meeting then the dendrites from another neuron. Besides this, it is clear how smaller dendrites enter inside the chitosan, as underlined by the black arrows. In Fig. 4C is reported a detail of the interface between cells and CHI microbeads, where many neurons components are evident: cell bodies, axons with distinct tubulin cytoskeleton, small dendrites, spines and synapses. From these two images, it is clear that on the microbeads surface there is a dense network made up of axons and dendrites of different size, while only the smaller dendrites penetrate into the CHI microbeads. In Fig. 4D is reported a detail of a dendrite taken far from the microbead surface (about 15 μm). The size of these terminations is smaller (<400 nm), but they are clearly neural dendrites, as suggested by some details as the cytoskeleton and the vesicles.

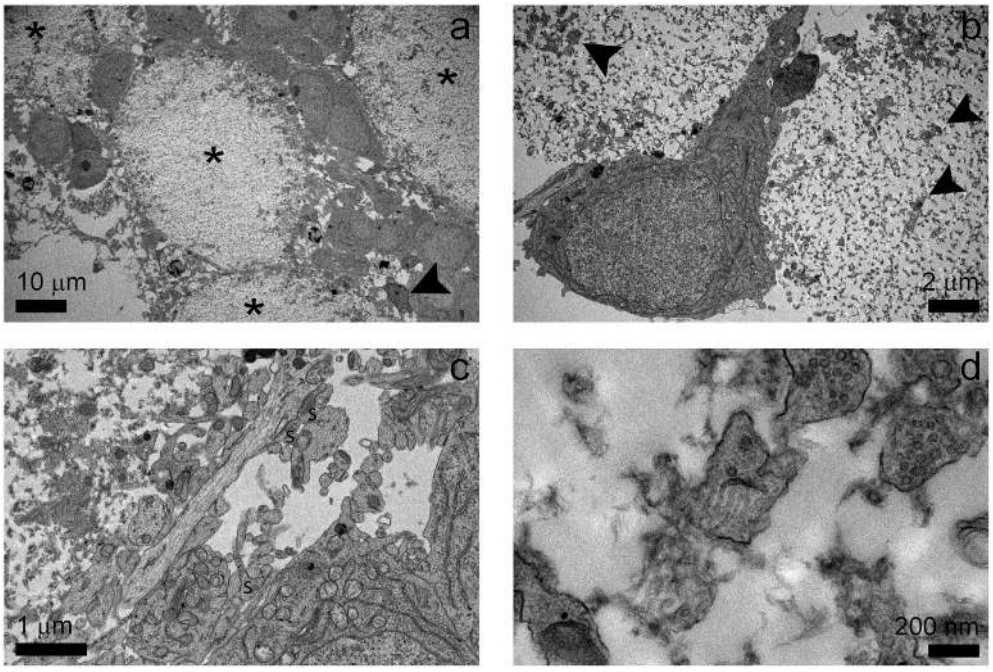


Fig. 4. Low-mag TEM micrograph of a portion of chitosan scaffold with the neuronal network: (A) CHI-microbeads are marked with the asterisks, while cells appear darker, the dark arrow highlight a glial cell. (B) A neuron grown between two microbeads (1000×). The dark arrows indicate dendrites inside the chitosan. (C) A detail (2500×) of the interface cell-CHI microbeads. Synapses are marked with the letter s. (D) High-mag (15000×) detail of dendrites taken far (15 μm) from the bead surface.

Indirect immunofluorescence techniques were then used to assess the *in vitro* morphological and functional cell behavior and to characterize the 3D structure of the network. To this purpose, after 25 DIVs, at the end of the recording sessions (see section 3.3), 3D cell-scaffolds were fixed with PFA 4% and labeled by using a panel of *ad-hoc* selected antibody molecules. The 3D neural networks were then characterized by confocal microscopy on MAP2 labeled neurons (Supplementary Movie 1) and on MAP-2 and Tubulin βIII (Supplementary Movie 2). Overall, the thickness of the 3D neuronal network on the 2% CHI microbeads was evaluated to be around 300–500 μm.

Supplementary video related to this article can be found at https://doi.org/10.1016/j.biomaterials.2017.11.043.

Fig. 5 shows the neuronal network development around the CHI microbeads (A, C) and around glass microbeads (B).

We can see (Fig. 5A, left and middle) neuronal soma from which rich neuritic arborizations depart. This is particularly evident around the CHI microbead surfaces while it becomes partially fragmented due to the penetration of neurites into the microporous volume of the microbeads (white arrows) (Supplementary Movie 3 and Movie 4). In the case of the glass microbeads, the neuronal network development was confined onto the surface of microbeads, without any fragmentation (Fig. 5B, left). Moreover, the shape of the soma was found to be spherical in both cases (Fig. 5 A–B, middle), as the one observed *in vivo* [25,64]. Fig. 5A (right) shows a section of the 3D culture where it is possible to observe the close assembly between CHI microbeads mediated by neuronal cells. Instead, in the case of glass microbeads a hexagonal structure was observed characterized by well-defined and separated microbeads (Fig. 5B, right). Fig. 5C left shows the structural proteins of the cytoskeleton of the 3D network on 2% CHI microbeads. Fig. 5C right shows the high density of synaptic puncta present on the 3D network.

Supplementary video related to this article can be found at https://doi.org/10.1016/j.biomaterials.2017.11.043.

In the formation of brain-like constructs a pivotal role in the survival and differentiation of neurons is played by glial cells [65]. In order to highlight the morphology of glia cells, fixed 3D and 2D cultures were exposed to GFAP primary antibody followed by secondary antibody Alexa Fluor 549.

It can be observed that the GFAP positive cells cultured both on 2D film and 3D microbeads 2% CHI (Fig. 6A–B) present a different morphology compared to GFAP positive cells cultured at the same conditions but on the 2D petri dish surface (Fig. 6C).

These results suggest that the chemical and mechanical environments play a relevant role on the morphological behavior. Similar observations were already reported in previous works [23,66–70].

The 3D structure of neuronal networks after 24 days of culture fixed and immunolabeled for the dendritic marker MAP-2 is illustrated in Fig. 7. Both the 3D reconstruction of 148 μm z-stack of the hippocampal network and the projections along different axes are shown, thus giving a comprehensive view of the neuronal network onto the CHI microbeads scaffold (Fig. 7B). The max intensity projection of the orthogonal view is represented in this figure: XZ projection (Fig. 7A) shows CHI microbeads profiles wrapped by neuronal network; Fig. 7C and D shows XY − YZ projections.

3.4. Functional characterization of 3D networks

In order to perform the electrophysiological characterization of the 3D networks grown onto CHI microbeads and to compare the obtained results with the ones reported in Ref. [25], CHI microbeads were pre-treated with a. p., then mixed with neurons and finally plated onto MEA. As reported in Ref. [25], before this final step, a 2D neuronal network was directly coupled to the active area of MEA in order to establish a good communication between the 3D culture and the underlying microelectrodes.

Fig. 8A shows the spontaneous activity (raw signal) of 10 s of a 3D CHI network as recorded from one microelectrode and characterized

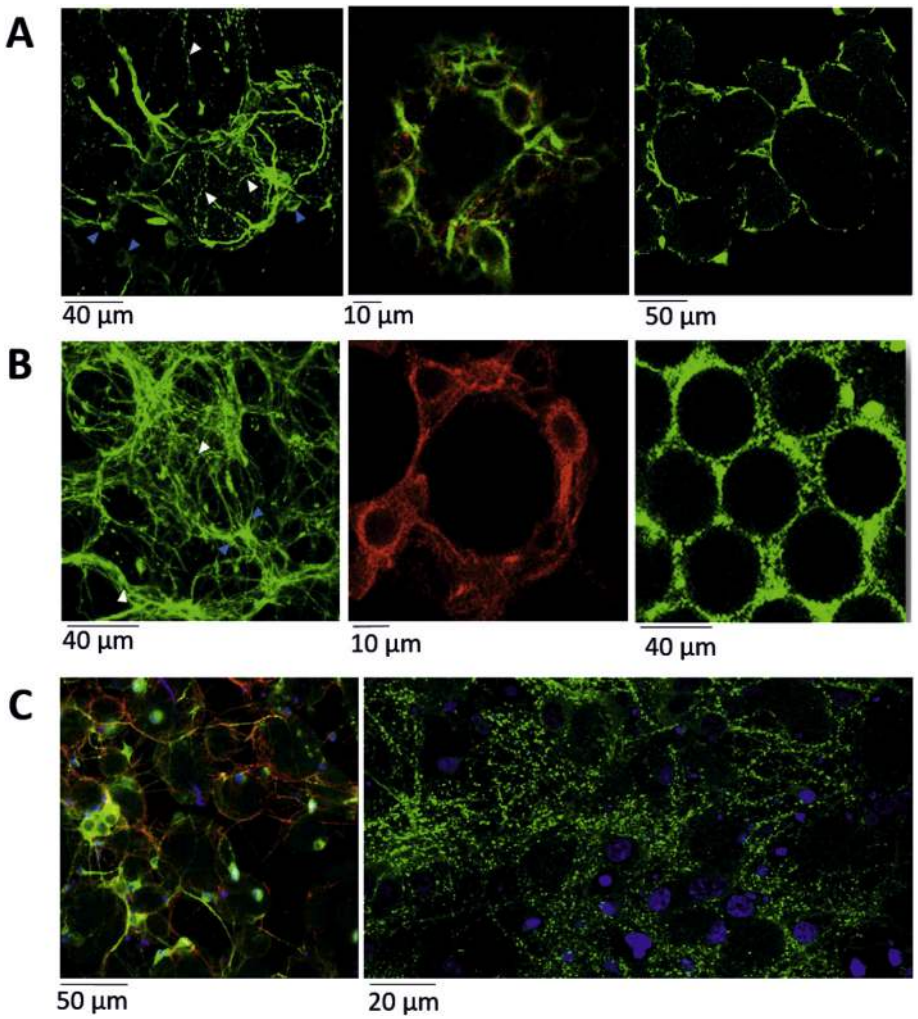


Fig. 5. Confocal microscope images of 3D neural network at DIV 25: (**A**) 3D neural network on 2% CHI microbeads (left), single 2% CHI microbead surrounded by almost six neurons (middle) and a section of 3D neural network on 2% CHI microbeads (right), MAP-2 (green) and Synapsin (red). (**B**) 3D neuronal network on glass microbeads (left), single glass microbead surrounded by five neurons (middle) and a section of 3D neural network on glass microbeads (right), MAP-2 (green and red). The blue arrows point the cell soma while the white one points neuritic fragmentation. (**C**) 3D neural network on 2% CHI microbeads (left) labeled for MAP-2 (green), Tubulin βIII (red) and DAPI (blu), 3D neural network on 2% CHI microbeads (right) labeled for Synapsin (green) and DAPI (blue). (For interpretation of the references to colour in this figure legend, the reader is referred to the web version of this article.)

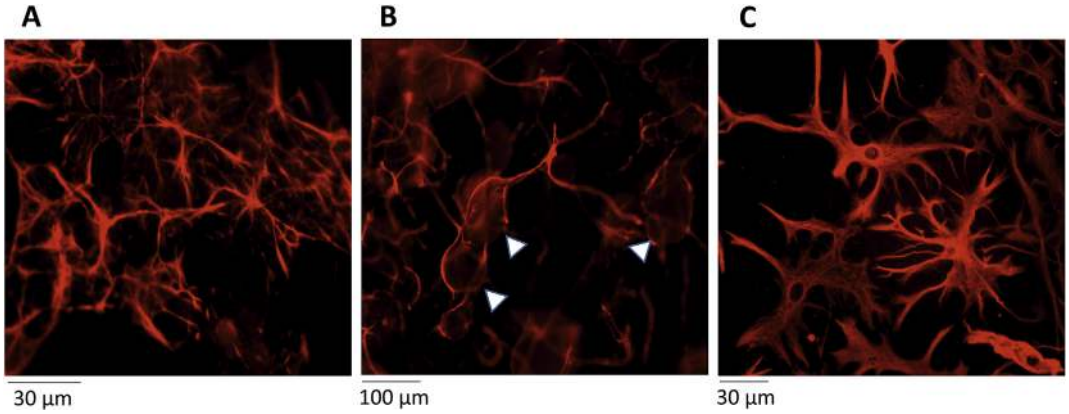


Fig. 6. Optical images of glial cells labeled for GFAP (DIV 25): (**A**) 2D network on CHI film; (**B**) 3D network on 2% CHI microbeads; (**C**) 2D network on petri dish. The white arrows point CHI microbeads.

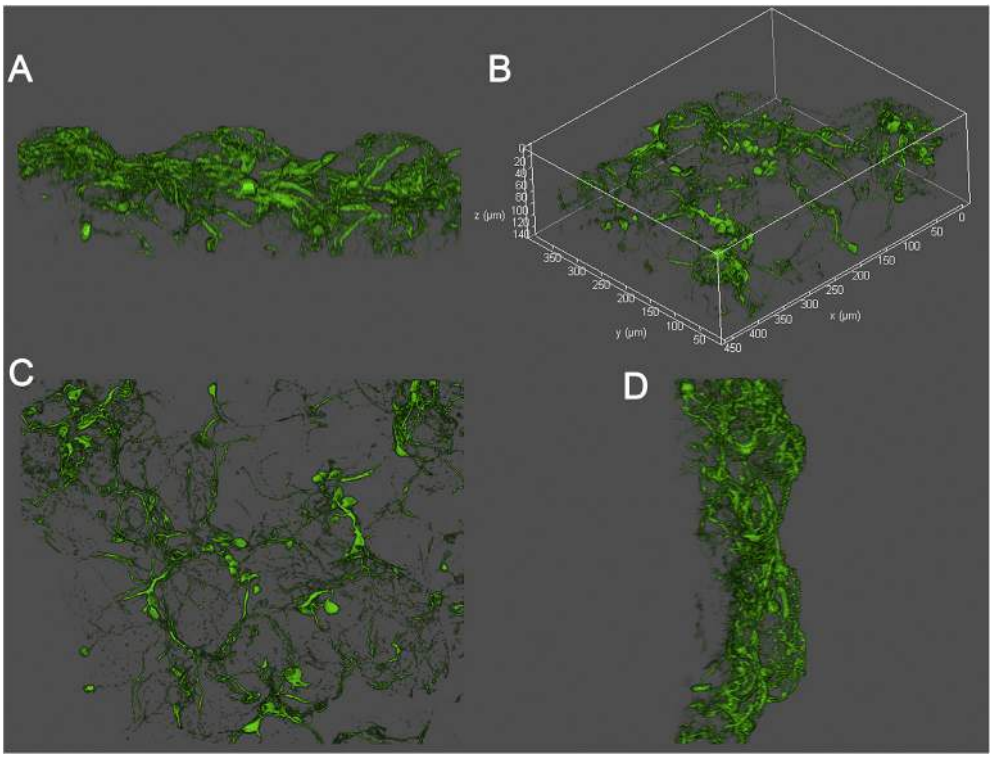


Fig. 7. Max intensity projection Orthogonal View and Rendering 3D of population neurons network on the scaffold labeled (DIV 24) for MAP-2: Cross-sectioning along different axes XZ (**A**), XY(**C**), YZ (**D**); (**B**) Volumetric representation (XYZ) of neuronal networks from the same sample.

by two bursts and random spikes. The global electrophysiological behavior of representative 3D networks, is qualitatively showed in the raster plots of Fig. 8B and C, where 300 s of spontaneous activity are displayed. In both experimental conditions (CHI, Fig. 8B and glass microbeads, Fig. 8C), quasi-synchronous network bursts (NB) are mixed with random spiking activity. However, 3D networks with CHI microbeads scaffold exhibit a global activity characterized by longer bursts than glass microbeads ones. After 21 DIV, we recorded 30 min of spontaneous activity of n = 3 CHI 1% networks, and n = 3 CHI 2% networks, and we compared the obtained results to n = 3 cultures where the 3D scaffold was realized by means of glass microbeads (Supplementary Materials Table S2). Fig. 8D–I shows the parameters extracted from the analyzed spike data. CHI 1% networks presented values of MFR (2.3 ± 0.14 spikes/s), statistically different from the CHI 2% ones (0.86 ± 0.05 spikes/s; $p < 0.001$) but similar to the MFR of the 3D glass microbeads networks (2.97 ± 0.55 spikes/s). All the 3D experimental configurations display high values of random spiking activity (Fig. 8E): specifically, CHI 1% and 2% networks show higher (statistically significant) values with respect to glass microbeads ones. Regarding the bursting behavior, the MBR of CHI 2% networks showed the lowest value (3.74 ± 0.31 (bursts/min)) which is significantly different ($p < 0.001$) from the CHI 1% and glass microbeads networks. On the other way, round (Fig. 8G), CHI 1% networks exhibited a MBD (310.5 ± 18.19 (ms)) significantly higher ($p < 0.001$) than the other two configurations that share similar MBD values (175.10 ± 16.41 ms and 190.70 ± 10.53 ms for CHI 2% and glass microbeads).

Finally, the NB activity was investigated by computing the network mean bursting rate (NBR; Fig. 8H) and duration (NBD; Fig. 8I). NBR was similar for CHI 1% and glass microbeads networks and statistically different with respect to CHI 2% networks. Again, for the NBD, CHI 1%, was different from CHI 2% and glass microbeads that are in turn characterized by shorter bursts (0.32 ± 0.036 s and 0.43 ± 0.067 s, respectively).

4. Discussion

4.1. Characterization of CHI microbeads

In this work, we explored the use of CHI microbeads to actively support 3D functional neuronal cultures. CHI was chosen for its biocompatibility, biodegradability, and low cost [6]. Moreover, in the literature it is reported that the positive charges of primary amines onto the polymer backbone favor the electrostatic interaction with the negatively charged cell membranes [42,44,71,72], promoting cell adhesion and growth.

In general, the stiffness, porosity, and electrostatic charge of the scaffold concur in neuritic development and extension. In our case, the stiffness of 1% CHI microbeads was found to be comparable to that of brain tissue (Fig. 2D). A difference in the stiffness, among 1% and 2% CHI microbeads, was observed and could be attributed to the increase in the concentration of CHI, corresponding to an increase in the density of the polymeric chains. Therefore, higher ionic interactions between the CHI chains seem to be quite predictable, as the concentration of chitosan increased from 1% to 2% [73]. Besides, as shown by water content result, microbeads with lower concentration of chitosan have a higher content of water which consequently caused a decrease in stiffness [74] However, this effect is not a major factor because the difference of water content in the two samples is not remarkable and it is logic to state that the increase in the ionic interactions is the main mechanism for the stiffness growth.

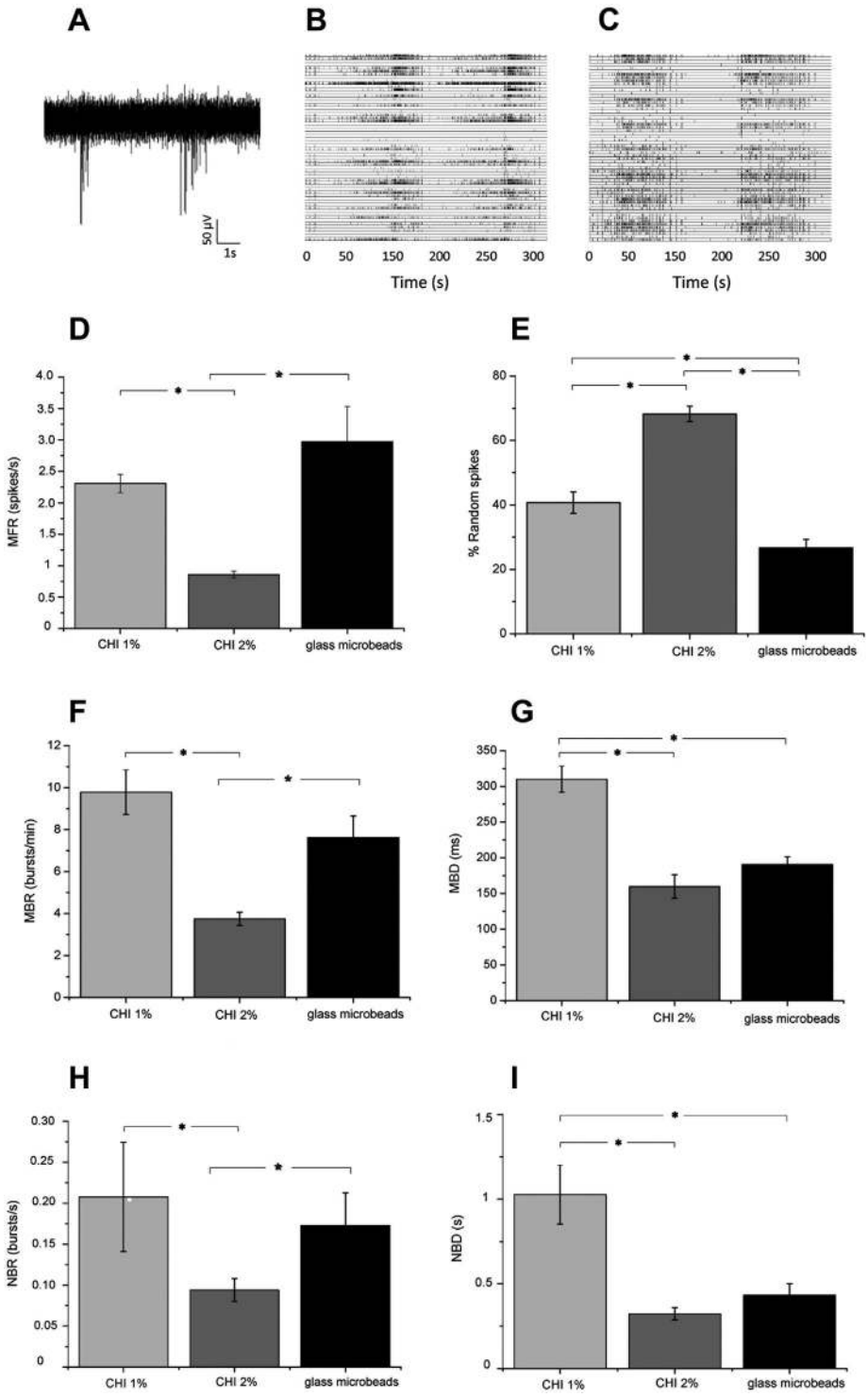


Fig. 8. Spontaneous activity characterization: (**A**) 10 s of raw data recorded from a single microelectrode. Raster plot showing 300 s of spontaneous activity of 3D network on (**B**) CHI 1% microbeads and(**C**) on glass bead; (**D**) mean firing rate, (**E**) percentage of random spiking activity, (**F**) mean bursting rate, (**G**) mean burst duration, (**H**) network bursting rate, (**I**) network bursts duration. (Kruskal-Wallis, $^{*}p \leq 10^{-3}$).

Finally, AFM revealed darker areas on the surface, which might represent holes whose apparent dimensions are in agreement with data obtained by TEM (see Section 4.3). (Fig. 2C). These characteristics combined with bioaffinity of CHI, due to the presence of primary amines, contributed to the formation of a dense neuronal network onto CHI microbeads.

4.2. Characterization of 2D neuronal networks on CHI films

In the effort of investigating the intrinsic bioaffinity of CHI, we firstly characterized its ability to induce cell attachment and neurite outgrowth without any pre-treatment with a. p. As a first step, this characterization was carried out using standard 2D cell culture

models onto the surface of CHI films. Quite surprisingly, non-pre-treated CHI films were able to support neuronal growth during a period of more than 15 days.

A similar observation was previously done for soft alginate hydrogels, which were able to support neural cell cultures in monolayer or spheroids [75,76]. However, the use of alginate as supporting material for neuronal cultures is controversial, since it requires Ca^{2+} ions for its ionic cross-linking and it is well known that neurons and glial cells are extremely sensitive to Ca^{2+} ions, even at nM concentrations [77].

To our knowledge, this is the first work reporting the ability of pure CHI to support neuronal cell attachment and functional neuronal network development. This represents a valuable contribution in the search for low-cost biomimetic culture systems, which can have important applications in neuropharmacology, toxicology, and regenerative medicine [78,79].

4.3. Characterization of 3D neuronal networks on CHI microbeads

The experimental design of this study was partially inspired by the results of a previous work in which a scaffold made by glass microbeads was used [25]. Indeed, to allow a direct comparison of results deriving from the use of CHI and glass microbeads, CHI microbeads were pre-treated with a. p. and employed as 3D support for cell attachment and growth.

The immunocytochemistry and confocal microscopy characterization allowed us to gain information on (i) the morphology of the 3D structure of mature neuronal networks after 24 days of culture and (ii) the distinct features of the two cell populations dissected from hippocampal rat brain tissues, namely neurons and glial cells.

Regarding cell morphology, the neuronal somata were found to be round, like the ones observed in the brain tissue. The ability of CHI microbeads to maintain the *in vivo* cell morphology was already reported by Garcia-Giralt et al., who studied their interaction with human chondrocytes [80].

This result underlines that the combination of different factors, including substrate stiffness, 3D arrangement, and chemical cues altogether contribute to support an *in vivo*-like growth of the neuronal network.

The scaffold topography, characterized by confocal microscopy, showed that while the micro-scale dendritic extensions were distributed on the external surface of the CHI microbeads, the nano-scale ones tended to penetrate the hydrogel, contributing to the formation of a compact structure.

This speculation was confirmed by TEM analysis, which allowed to understand in depth the micro- and nano-structure of the neuron-microbeads assembly. TEM micrographs (Fig. 4) clearly support the data obtained by confocal microscopy, putting in evidence that CHI microbeads are enveloped in a dense network of neural dendrites and axons. At the same time, we had the evidence that smaller dendrites are allowed to enter and spread inside the CHI microbeads, proving its porosity to neural dendrites.

The astrocyte glial fraction also proliferates on CHI microbeads and its morphology was again similar to the one found in brain tissue (i.e., having a thin morphology and expression in GFAP). This observation was already reported by others [67,68] for 3D *in vitro* cultures, thus suggesting a substrate-induced morphological dependence. Interestingly, also the morphology of glial cells cultured onto CHI film was found to be stretched (Fig. 6).

In the meanwhile, glial cells and the natural ECM, spontaneously produced by the neurons network in culture, were responsible for the assembly of the microbeads after four-weeks in culture. In order to verify the presence of natural ECM, we assessed the formation of perineuronal net-like structures in our culture systems using WFA (Supplementary Movie 5).

Supplementary video related to this article can be found at https://doi.org/10.1016/j.biomaterials.2017.11.043.

Finally, it is worth mentioning that no evident differences between the microbeads made by CHI at 1% compared to those at 2% were observed in terms of neuronal morphology and distribution of the biological material on the scaffold.

4.4. Functional characterization of 3D neuronal networks on CHI microbeads

Regarding the electrophysiological characterization, after 21 DIVs, the 3D neuronal networks developed onto CHI microbeads presented electrophysiological patterns similar to the ones observed for the glass microbeads in terms of the percentage of random spiking and bursting behavior. As already observed by Frega et al. [25] in the case of glass microbeads, the percentage of random spiking of the 3D CHI networks presents higher values than those observed in 2D cultures (Supplementary materials Fig. S4). Here we found a further increase of random spiking with respect to the 3D glass microbead networks. Moreover, we observed that 3D CHI 1% networks show more synchronous bursts (MBR, NBR), with respect to 3D CHI 2% with associated longer duration for both bursts and network bursts. This activity indicates the formation of a very dense network with a high degree of connectivity as also suggested by the immunostaining for Synapsin (Fig. 5C right) and for MAP-2 (Fig. 7). Therefore, the 3D CHI model presents possible advantages that would merit further investigations: (i) stiffness similar to the living brain tissue; (ii) no need for pre-treatment with a. p.; (iii) high-level of connectivity; (iv) *in vivo* like electrophysiological behavior.

From the other side, it should be considered that the number of active electrodes was significantly lower in the case of CHI microbeads based 3D cultures. This was due to a lack of contacts between MAE surface and the overhanging 3D assembly. Neurons, cultured on the MEA surface, were partially transferred from the 2D monolayer to the surface of the overhanging 3D assembly. This was probably due to the higher bioaffinity of CHI than MEA surface. Moreover, it should be considered that we observed a stable assembly between CHI microbeads and cells only after the first week in culture. Therefore, the mechanical stresses caused by replacements of the medium in the first week of culture might have contributed to the weakening of the 3D assembly.

Arrays of 3D microelectrodes ad hoc designed would provide easier physical integration with the culture and more resolved access to the electrophysiological network activity.

5. Conclusions

Chitosan microbeads based scaffolds were specifically optimized and adapted in order to be integrated onto planar MEAs to study and better understand the functional properties of biomimetic 3D hippocampal networks. Chitosan microbeads both treated and untreated with adhesion factors were tested and both of them proved to be reliable supports, able to sustain the neuronal population during the growth in a 3D space. At the same time, the chitosan microbeads guaranteed both a morphological and structural development of a functional network. Finally, we demonstrated that the neuronal network itself was responsible for the assembly and the stabilization of the 3D chitosan based structure. In conclusion, CHI seems to be a promising scaffolding-support for developing 3D neuronal networks towards the design and implementation of brain-on-a-chip microsystems.

Funding

This research did not receive any specific grant from funding agencies in the public, commercial, or not-for-profit sectors.

Acknowledgements

Maria Concetta Miniaci for her valuable comments on this work and Giorgio Carlini for the technical support.

Appendix A. Supplementary data

Supplementary data related to this article can be found at https://doi.org/10.1016/j.biomaterials.2017.11.043.

References

[1] T. Dvir, et al., Nanotechnological strategies for engineering complex tissues, Nat. Nanotechnol. 6 (1) (2011) 13–22.
[2] E. Cukierman, et al., Taking cell-matrix adhesions to the third dimension, Science 294 (5547) (2001) 1708–1712.
[3] B.A. Justice, N.A. Badr, R.A. Felder, 3D cell culture opens new dimensions in cell-based assays, Drug Discov. Today 14 (1–2) (2009) 102–107.
[4] L.G. Griffith, M.A. Swartz, Capturing complex 3D tissue physiology in vitro, Nat. Rev. Mol. Cell Biol. 7 (3) (2006) 211–224.
[5] F. Pampaloni, E.G. Reynaud, E.H. Stelzer, The third dimension bridges the gap between cell culture and live tissue, Nat. Rev. Mol. Cell Biol. 8 (10) (2007) 839–845.
[6] D.B. Kolesky, et al., 3D bioprinting of vascularized, heterogeneous cell-laden tissue constructs, Adv. Mater. 26 (19) (2014) 3124–3130.
[7] K.H. Benam, et al., Engineered in vitro disease models, Annu. Rev. Pathol. 10 (2015) 195–262.
[8] D. Huh, et al., Microfabrication of human organs-on-chips, Nat. Protoc. 8 (11) (2013) 2135–2157.
[9] B. Weigelt, C.M. Ghajar, M.J. Bissell, The need for complex 3D culture models to unravel novel pathways and identify accurate biomarkers in breast cancer, Adv. Drug Deliv. Rev. 69–70 (2014) 42–51.
[10] J. Lee, et al., In vitro toxicity testing of nanoparticles in 3D cell culture, Small 5 (10) (2009) 1213–1221.
[11] M.W. Tibbitt, K.S. Anseth, Hydrogels as extracellular matrix mimics for 3D cell culture, Biotechnol. Bioeng. 103 (4) (2009) 655–663.
[12] S. Breslin, L. O'Driscoll, Three-dimensional cell culture: the missing link in drug discovery, Drug Discov. Today 18 (5–6) (2013) 240–249.
[13] A. Roth, T. Singer, The application of 3D cell models to support drug safety assessment: opportunities & challenges, Adv. Drug Deliv. Rev. 69–70 (2014) 179–189.
[14] M.J. Mahoney, K.S. Anseth, Three-dimensional growth and function of neural tissue in degradable polyethylene glycol hydrogels, Biomaterials 27 (10) (2006) 2265–2274.
[15] L.S. Wang, et al., Injectable biodegradable hydrogels with tunable mechanical properties for the stimulation of neurogenesic differentiation of human mesenchymal stem cells in 3D culture, Biomaterials 31 (6) (2010) 1148–1157.
[16] A. Kunze, et al., Micropatterning neural cell cultures in 3D with a multi-layered scaffold, Biomaterials 32 (8) (2011) 2088–2098.
[17] D.R. Nisbet, et al., Neural tissue engineering of the CNS using hydrogels, J. Biomed. Mater. Res. Part B Appl. Biomater. 87 (1) (2008) 251–263.
[18] S.R. Caliari, J.A. Burdick, A practical guide to hydrogels for cell culture, Nat. Methods 13 (5) (2016) 405–414.
[19] A.S. Hoffman, Hydrogels for biomedical applications, Ann. N. Y. Acad. Sci. 944 (2001) 62–73.
[20] Y. Du, et al., Directed assembly of cell-laden microgels for fabrication of 3D tissue constructs, Proc. Natl. Acad. Sci. U. S. A. 105 (28) (2008) 9522–9527.
[21] C.M. Magin, D.L. Alge, K.S. Anseth, Bio-inspired 3D microenvironments: a new dimension in tissue engineering, Biomed. Mater. 11 (2) (2016) 022001.
[22] S. Pautot, C. Wyart, E.Y. Isacoff, Colloid-guided assembly of oriented 3D neuronal networks, Nat. Methods 5 (8) (2008) 735–740.
[23] T.B. Puschmann, et al., A novel method for three-dimensional culture of central nervous system neurons, Tissue Eng. Part C Methods 20 (6) (2014) 485–492.
[24] S. Bosi, et al., From 2D to 3D: novel nanostructured scaffolds to investigate signalling in reconstructed neuronal networks, Sci. Rep. 5 (2015) 9562.
[25] M. Frega, et al., Network dynamics of 3D engineered neuronal cultures: a new experimental model for in-vitro electrophysiology, Sci. Rep. 4 (2014) 5489.
[26] J. Lantoine, et al., Matrix stiffness modulates formation and activity of neuronal networks of controlled architectures, Biomaterials 89 (2016) 14–24.
[27] I. Levental, P.C. Georges, P.A. Janmey, Soft biological materials and their impact on cell function, Soft Matter. 3 (3) (2007) 299–306.
[28] A.P. Balgude, et al., Agarose gel stiffness determines rate of DRG neurite extension in 3D cultures, Biomaterials 22 (10) (2001) 1077–1084.
[29] M. Antman-Passig, O. Shefi, Remote magnetic orientation of 3D collagen hydrogels for directed neuronal regeneration, Nano Lett. 16 (4) (2016) 2567–2573.
[30] D. Ge, et al., Culture and differentiation of rat neural stem/progenitor cells in a three-dimensional collagen scaffold, Appl. Biochem. Biotechnol. 170 (2) (2013) 406–419.
[31] M. Uemura, et al., Matrigel supports survival and neuronal differentiation of grafted embryonic stem cell-derived neural precursor cells, J. Neurosci. Res. 88 (3) (2010) 542–551.
[32] J.P. Frampton, et al., Fabrication and optimization of alginate hydrogel constructs for use in 3D neural cell culture, Biomed. Mater 6 (1) (2011) 015002.
[33] N. Broguiere, L. Isenmann, M. Zenobi-Wong, Novel enzymatically cross-linked hyaluronan hydrogels support the formation of 3D neuronal networks, Biomaterials 99 (2016) 47–55.
[34] M. Matyash, et al., Swelling and mechanical properties of alginate hydrogels with respect to promotion of neural growth, Tissue Eng. Part C Methods 20 (5) (2014) 401–411.
[35] K.E. Crompton, et al., Polylysine-functionalised thermoresponsive chitosan hydrogel for neural tissue engineering, Biomaterials 28 (3) (2007) 441–449.
[36] PattersonJ. et al., Biomimetic materials in tissue engineering. Mater. Today, 13(1), 14–22;
[37] J.A. Hunt, et al., Hydrogels for tissue engineering and regenerative medicine, J. Mater. Chem. B 2 (33) (2014) 5319–5338.
[38] R. Lozano, et al., 3D printing of layered brain-like structures using peptide modified gellan gum substrates, Biomaterials 67 (2015) 264–273.
[39] N.D. Leipzig, M.S. Shoichet, The effect of substrate stiffness on adult neural stem cell behavior, Biomaterials 30 (36) (2009) 6867–6878.
[40] S. Wrobel, et al., In vitro evaluation of cell-seeded chitosan films for peripheral nerve tissue engineering, Tissue Eng. Part A 20 (17–18) (2014) 2339–2349.
[41] N.B. Skop, et al., Optimizing a multifunctional microsphere scaffold to improve neural precursor cell transplantation for traumatic brain injury repair, J. Tissue Eng. Regen. Med. 10 (10) (2016) E419–E432.
[42] C.M. Valmikinathan, et al., Photocrosslinkable chitosan based hydrogels for neural tissue engineering, Soft Matter. 8 (6) (2012) 1964–1976.
[43] S. Guan, et al., Chitosan/gelatin porous scaffolds containing hyaluronic acid and heparan sulfate for neural tissue engineering, J. Biomater. Sci. Polym. Ed. 24 (8) (2013) 999–1014.
[44] Z. Cao, R.J. Gilbert, W. He, Simple agarose-chitosan gel composite system for enhanced neuronal growth in three dimensions, Biomacromolecules 10 (10) (2009) 2954–2959.
[45] C.Y. Sung, et al., Probing neural cell behaviors through micro-/nano-patterned chitosan substrates, Biofabrication 7 (4) (2015) 045007.
[46] C. Huang, et al., The migration and differentiation of hUC-MSCs(CXCR4/GFP) encapsulated in BDNF/chitosan scaffolds for brain tissue engineering, Biomed. Mater. 11 (3) (2016) 035004.
[47] M. Rinaudo, Chitin and chitosan: properties and applications, Prog. Polym. Sci. 31 (7) (2006) 603–632.
[48] T. Kean, M. Thanou, Biodegradation, biodistribution and toxicity of chitosan, Adv. Drug. Deliv. Rev. 62 (1) (2010) 3–11.
[49] A. Anitha, et al., Chitin and chitosan in selected biomedical applications, Prog. Polym. Sci. 39 (9) (2014) 1644–1667.
[50] J.M. Zuidema, et al., Fabrication and characterization of tunable polysaccharide hydrogel blends for neural repair, Acta Biomater. 7 (4) (2011) 1634–1643.
[51] M. Dash, et al., Chitosan—a versatile semi-synthetic polymer in biomedical applications, Prog. Polym. Sci. 36 (8) (2011) 981–1014.
[52] C.A. Custódio, et al., Functionalized microparticles producing scaffolds in combination with cells, Adv. Funct. Mater. 24 (10) (2014) 1391–1400.
[53] Q. He, et al., Preparation of chitosan films using different neutralizing solutions to improve endothelial cell compatibility, J. Mater. Sci. Mater. Med. 22 (12) (2011) 2791–2802.
[54] J. Du, et al., Comparative evaluation of chitosan, cellulose acetate, and polyethersulfone nanofiber scaffolds for neural differentiation, Carbohydr. Polym. 99 (2014) 483–490.
[55] G.M. Pharr, W.C. Oliver, F.R. Brotzen, On the generality of the relationship among contact stiffness, contact area, and elastic modulus during indentation, J. Mater. Res. 7 (3) (2011) 613–617.
[56] E. Defranchi, et al., Imaging and elasticity measurements of the sarcolemma of fully differentiated skeletal muscle fibres, Microsc. Res. Tech. 67 (1) (2005) 27–35.
[57] G.J. Brewer, C.W. Cotman, NMDA receptor regulation of neuronal morphology in cultured hippocampal neurons, Neurosci. Lett. 99 (1989) 268–273.
[58] M. Tedesco, et al., Interfacing 3D engineered neuronal cultures to microelectrode arrays: an innovative in vitro experimental model, JoVE (104) (2015) e53080.
[59] L.L. Bologna, et al., Investigating neuronal activity by SPYCODE multi-channel data analyzer, Neural Netw. 23 (6) (2010) 685–697.
[60] A. Maccione, et al., A novel algorithm for precise identification of spikes in extracellularly recorded neuronal signals, J. Neurosci. Methods 177 (1) (2009) 241–249.
[61] V. Pasquale, S. Martinoia, M. Chiappalone, A self-adapting approach for the detection of bursts and network bursts in neuronal cultures, J. Comput. Neurosci. 29 (1) (2010) 213–229.
[62] A.J. Engler, et al., Matrix elasticity directs stem cell lineage specification, Cell 126 (4) (2006) 677–689.

[63] L.A. Flanagan, et al., Neurite branching on deformable substrates, Neuroreport 13 (18) (2002) 2411–2415.
[64] D.K. Cullen, et al., Neural tissue engineering and biohybridized microsystems for neurobiological investigation in vitro (Part 1), Crit. Rev. Biomed. Eng. 39 (3) (2011) 201–240.
[65] A. Verkhratsky, Physiology of neuronal–glial networking, Neurochem. Int. 57 (4) (2010) 332–343.
[66] P.M.D. Watson, et al., Bioengineered 3D glial cell culture systems and applications for neurodegeneration and neuroinflammation, SLAS Discov. 22 (5) (2017) 583–601.
[67] I. Smith, et al., Neuronal-glial populations form functional networks in a biocompatible 3D scaffold, Neurosci. Lett. 609 (2015) 198–202.
[68] T.B. Puschmann, et al., Bioactive 3D cell culture system minimizes cellular stress and maintains the in vivo-like morphological complexity of astroglial cells, Glia 61 (3) (2013) 432–440.
[69] S. Balasubramanian, et al., Three-Dimensional environment sustains morphological heterogeneity and promotes phenotypic progression during astrocyte development, Tissue Eng. Part A 22 (11–12) (2016) 885–898.
[70] A.L. Placone, et al., Human astrocytes develop physiological morphology and remain quiescent in a novel 3D matrix, Biomaterials 42 (2015) 134–143.
[71] V.I. Scanga, et al., Biomaterials for neural-tissue engineering — chitosan supports the survival, migration, and differentiation of adult-derived neural stem and progenitor cells, Can. J. Chem. 88 (3) (2010) 277–287.
[72] M. Prasitsilp, et al., Cellular responses to chitosan in vitro: the importance of deacetylation, J. Mater Sci. Mater Med. 11 (12) (2000) 773–778.
[73] Dabiri, Seyed Mohammad Hossein, et al., New in-situ synthetized hydrogel composite based on alginate and brushite as a potential pH sensitive drug delivery system, Carbohydr. Polym. 177 (2017) 324–333.
[74] Seung G. Lee, et al., Molecular dynamics simulation study of P (VP-co-HEMA) hydrogels: effect of water content on equilibrium structures and mechanical properties, Biomaterials 30.30 (2009) 6130–6141.
[75] G. Palazzolo, et al., Ultrasoft alginate hydrogels support long-term three-dimensional functional neuronal networks, Tissue Eng. Part A 21 (15–16) (2015) 2177–2185.
[76] M. Matyash, et al., Novel soft alginate hydrogel strongly supports neurite growth and protects neurons against oxidative stress, Tissue Eng. Part A 18 (1–2) (2012) 55–66.
[77] C. Agulhon, et al., What is the role of astrocyte calcium in neurophysiology? Neuron 59 (6) (2008) 932–946.
[78] S.S. Lim, D.C. Foo, Simulation and scale-up study for a chitosan–TiO2 nanotubes scaffold production, Food Bioprod. Process. 106 (2017) 108–116.
[79] I. Hamed, et al., Industrial applications of crustacean by-products (chitin, chitosan, and chitooligosaccharides): a review, Trend. Food Sci. Technol. 48 (2016) 40–50.
[80] N. Garcia-Giralt, et al., Chitosan microparticles for “in vitro” 3D culture of human chondrocytes 3 (2013) 6362–6368.